Linking transcriptional and genetic tumor heterogeneity through allele analysis of single-cell RNA-seq data

Jean Fan[1,*], Hae-Ock Lee[2,*], Soohyun Lee[1], Da-eun Ryu[2], Semin Lee[1], Catherine Xue[1], Seok Jin Kim[5], Kihyun Kim[5], Nikolaos Barkas[1], Peter J. Park[1], Woong-Yang Park[2,§], Peter V. Kharchenko[1,3,4,§]

Affiliations

[1] Department of Biomedical Informatics, Harvard Medical School, Boston, MA, USA

[2] Samsung Genome Institute, Samsung Medical Center/Sungkyunkwan University School of Medicine, Seoul, Korea

[3] Hematology/Oncology Program, Children's Hospital, Boston, Massachusetts, USA

[4] Harvard Stem Cell Institute, Cambridge, Massachusetts, USA

[5] Division of Hematology-Oncology, Department of Medicine, Sungkyunkwan University School of medicine, Samsung Medical Center, Seoul, Korea

* these authors contributed equally to this study

[§] Correspondence should be addressed to: PVK (peter_kharchenko@hms.harvard.edu) and WYP (woongyang.park@samsung.com)

Running title: single cell allele-based CNV inference

Key words: single cells, bioinformatics, intratumoral heterogeneity

ABSTRACT

Characterization of intratumoral heterogeneity is critical to cancer therapy, as presence of phenotypically diverse cell populations commonly fuels relapse and resistance to treatment. Although genetic variation is a well-studied source of intratumoral heterogeneity, the functional impact of most genetic alterations remains unclear. Even less understood is the relative importance of other factors influencing heterogeneity, such as epigenetic state or tumor microenvironment. To investigate the relationship between genetic and transcriptional heterogeneity in a context of cancer progression, we devised a computational approach called HoneyBADGER to identify copy number variation and loss-of-heterozygosity in individual cells from single-cell RNA-sequencing data. By integrating allele and normalized expression information, HoneyBADGER is able to identify and infer the presence of subclone-specific alterations in individual cells and reconstruct underlying subclonal architecture. Examining several tumor types, we show that HoneyBADGER is effective at identifying deletion, amplifications, and copy-neutral loss-of-heterozygosity events, and is capable of robustly identifying subclonal focal alterations as small as 10 megabases. We further apply HoneyBADGER to analyze single cells from a progressive multiple myeloma patient to identify major genetic subclones that exhibit distinct transcriptional signatures relevant to cancer progression. Surprisingly, other prominent transcriptional subpopulations within these tumors did not line up with the genetic subclonal structure, and were likely driven by alternative, non-clonal mechanisms. These results highlight the need for integrative analysis to understand the molecular and phenotypic heterogeneity in cancer.

INTRODUCTION

Intra-tumor heterogeneity is a common feature across diverse cancer types. Dynamic changes among intra-tumoral subpopulations over time and following therapy, presents a key challenge to current standards of cancer treatment (Gerlinger et al. 2012; Wu 2012; Mroz et al. 2015; Ding et al. 2012; Shah et al. 2012). Genetic variation such as copy number alterations is a well-studied source of intratumoral heterogeneity (Melchor et al. 2014; Vogelstein et al. 2013). The extent to which such alterations are able to drive tumor development typically relies on specific expression dysregulation of tumor cells. While some of the alterations have been tied to perturbations of known oncogenes and tumor suppressors, such as *MYC* and *TP53* (Glitza et al. 2015; Sekiguchi et al. 2014), the process by which many genetic alterations impact transcriptional processes to drive disease progression and drug resistance, particularly in combination, is not well understood (Lohr et al. 2014). In that regard, the ability to examine the transcriptional states of genetically distinct intratumoral subclones would be helpful for evaluating the likely functional impact of associated subclonal mutations. Such knowledge could help design rational strategies for development of new treatments, identify cellular pathways responsible for variable patient response or resistance to treatment, and could improve prognostic stratification and evaluation of therapeutic approaches (Walker et al. 2014).

While some insights into the relationship between genetic and transcriptional heterogeneity have been gained from bulk analysis, further characterization on the single-cell level is needed to more accurately dissect the pathway and regulatory features associated with distinct genetic subclones. Single-cell RNA-sequencing (scRNA-seq) methods can provide detailed information on the transcriptional state of the cancer cells. However, integration with genotypic information at the single-cell level is necessary to establish correspondence between transcriptionally distinct subpopulations and genetic subclones. At the same time, simultaneous unbiased assessment of DNA and RNA from an individual cell remains challenging (Macaulay et al. 2015; Dey et al. 2015; Wang et al. 2017).

Computational approaches for bulk sequencing data detect CNVs based on consistent deviations in read coverage as well as allelic imbalance within the region (Wang et al. 2007; Boeva et al. 2012; Chen et al. 2013). In the context of scRNA-seq, recent publications have used deviations in average expression magnitude within affected regions from a normal tissue reference to illustrate the presence of chromosome-scale CNVs (Patel et al. 2014; Tirosh et al. 2016). Likewise, analysis of allelic imbalance may also be informative about CNVs in the context of scRNA-seq. Here, we propose a computational approach called HoneyBADGER to quantitatively infer the presence of subclone-specific focal copy number variation (CNV) and loss of heterozygosity (LOH) events in individual cells using allele and expression information from scRNA-seq data.

RESULTS

Prevalence of mono-allelic detection in scRNA-seq data presents challenges

To evaluate whether sequence variant information available in the RNA reads can be used to distinguish subclones, we first examined the ability to detect single-nucleotide variants from scRNA-seq data. Using whole-exome sequencing (WES) to identify heterozygous single-nucleotide polymorphisms (SNPs) in the K562 cell line, we evaluated the sensitivity of detecting such SNPs from both bulk and single-cell RNA-seq K562 data (Fig. 1A). The average sensitivity for detecting covered SNPs (≥3 reads) in single-cell data was only 0.34, compared to 0.76 for the bulk RNA-seq data. Much of this difference can be attributed to the lower read coverage in single-cell data. However, sensitivity remains significantly lower even for well-covered SNPs (Fig. 1B). In such cases, all of the transcript reads detected originate from only one of the alleles. Like others, we find such mono-allelic detection to be prevalent in scRNA-seq data (Deng et al. 2014; Borel et al. 2015; Wang et al. 2017). Although the likelihood of observing both alleles generally increases with increasing level of gene expression, it remains low even for highly-expressed genes (Fig. 1B). This prevalence of this mono-allelic detection, a consequence of transcriptional stochasticity, sparse sampling of mRNA molecules, and subsequent uneven amplification by the scRNA-seq protocols (Deng et al. 2014), limits the confidence with which we can deduce the absence of a variant in a cell. This together with the sparse coverage characteristic of scRNA-seq data suggest that joint statistical analysis of many of variant sites is necessary to achieve genotype classification of cells.

HoneyBADGER identifies CNVs in single cells

Contiguous regions of variant sites are affected by focal heterozygous chromosomal deletions, amplifications, and LOH events in a coordinated manner (Fig. 1C). For example, if many SNPs across multiple genes within a putative deletion region are consistently expressed from the same allele in a given cell, then the cell likely harbors that deletion. Thus, joint analysis of heterozygous SNPs encompassed by such regions can overcome the uncertainty of individual SNPs detection. However, the number of SNPs and their associated read coverage must be sufficient to rule out the possibility of such allelic imbalance being observed by chance because of mono-

allelic detection. We therefore developed a hidden Markov model integrated Bayesian approach for detecting CNVs and LOHs from single-cell RNA-seq data (HoneyBADGER) to identify candidate CNV regions and perform joint statistical analysis of multiple SNPs within these regions to achieve genotype classification of cells (see Methods). HoneyBADGER employs a Bayesian approach to quantify the posterior probability of a CNV in each cell based on the observed allele ratios within the affected region, taking into consideration the expected prevalence of mono-allelic detection (Fig. 2, Methods).

As an initial step, HoneyBADGER identifies candidate CNV regions by a recursive hidden Markov model (HMM) approach (Fig. 2). Briefly, the allele frequency data is pooled across cells, and CNV-affected regions are identified by the HMM based on a consistent deviation of the allele fraction of heterozygous variants away from the expected 0.5 allele fraction. The presence of genetically distinct subpopulations, such as mixture of tumor and microenvironment, or different tumor subclones, decreases the sensitivity of the CNV detection step and the accuracy of the identified CNV boundaries. To handle such heterogeneous subpopulations, HoneyBADGER recursively clusters cells by similarity of their smoothed lesser allele fraction profile, where the lesser allele is defined as the allele that is less frequently observed across our population of cells. In the presence of a deletion, we expect to see persistent depletion of this lesser allele across our population of cells harboring the deletion. Where candidate CNVs of interest are known based on genomic sequencing or biological knowledge, such as common deletions spanning *TP53*, this candidate CNV discovery step with HMM may be skipped altogether. We note that the identity of the lesser allele implies phasing of haplotypes across multiple genes, beyond the phasing signal apparent from the mono-allelic detection within individual genes.

Then, for each candidate CNV region identified, HoneyBADGER evaluates the posterior probability that an individual cell harbors the alteration based on observed patterns of allelic imbalance using a Bayesian hierarchical framework (Fig. 2, Methods). This second layer of evaluation protects against false positives introduced in the HMM phase and takes into account potential uncertainty in phasing by reassessing the identity of the lesser allele using allele counts from individual cells rather than pooled frequencies. Based on the posterior probabilities for

these deletions, we then separate cells into genetic branches, and recursively search for additional subclonal alterations within each branch.

At a basic level, analysis of CNV/LOH occurrence by HoneyBADGER enables separation of tumor cells from karyotypically-normal cells. To demonstrate HoneyBADGER, we first examined 44 cells from serial bone marrow biopsies of a multiple myeloma (MM) patient. Twenty-three cells were analyzed from a biopsy obtained at diagnosis (MM16) with an estimated 90% purity and 21 cells were analyzed from a biopsy obtained 6 months later in a minimal disease state after chemotherapy (MM16R) with an estimated 10% purity based on $CD138^{+}$ expression. Using known heterozygous SNPs from previous bulk sequencing efforts, we identified multiple clonal whole-chromosome deletions (Fig. 3A, B). As expected due to the low purity in sample MM16R, only 5 of 21 cells (24%) originating from MM16R are inferred to be tumor cells, harboring all of the identified CNVs with high posterior probability (Fig. 3C). Similarly, 22 out of 23 cells (96%) originating from MM16 are inferred to be tumor. Thus, the percentage of putative normal and MM cells in MM16 and MM16R are consistent with bulk purity estimates. We validate identified deletions using FISH and cytogenetics (Fig. 3D) and bulk WES (Fig. 3E).

HoneyBADGER can further resolve focal CNVs previously that are not detectable by expression-based karyotyping approaches (Patel et al. 2014). Using scRNA-seq data from Patel et al. (Patel et al. 2014) , we applied HoneyBADGER to examine 65 glioblastoma (GBM) cells mixed with 10 normal cells from patient MGH31. We took advantage of the contamination of normal cells to identify heterozygous SNPs without reliance on additional sequencing data, such as WES. Briefly, we pooled all single cells from MGH31 and identified sites exhibiting multiple alleles. To avoid somatic alterations, we restricted SNP sites to known common population SNPs (MAF > 10%) from the ExAC database (Lek et al. 2016). HoneyBADGER recovers known deletions on Chromosome (Chr) 10, 13, and 14 (Supplemental Fig. 1A, B). Furthermore, it identifies an additional focal deletion (15Mbs) on Chr 19 with equal clonality to the deletion on Chr 10 (Supplemental Fig. 1A, B, C, Supplemental Table 1). Given relatively small size of this deletion, it could not be detected using expression-based karyotyping (Supplemental Fig. 1D), highlighting increased sensitivity of the allele-based approach. We note that even without presence of

karyotypically normal cells to assist with the identification of heterozygous SNPs, our approach is still able to identify clonal deletions based on a significant depletion of common heterozygous SNPs from the ExAC database on Chr 10 compared to other regions of comparable size and gene density (Supplemental Fig. 2A-B).

To assess the performance of HoneyBADGER on CNVs of varying size and clonality, we simulated deletions of varying size and clonality by inserting fragments of known deletions into CNV-neutral regions in MGH31 (see Methods). These simulations suggest that HoneyBADGER can accurately identify and resolve clonal deletions as small as 10Mbs in size (Fig. 4A), as well as chromosome-arm-level subclonal deletions present in as few as 30% of cells (Fig. 4B, Supplemental Fig. 2C-D).

While the benchmarks thus far have focused on full-transcript-coverage scRNA-seq data produced using the Smart-seq2 protocol (Picelli et al. 2014)., newer droplet microfluidic protocols that sequence only the 3'-end of transcripts are becoming increasingly common (Klein et al. 2015; Macosko et al. 2015). To assess the utility of our allele-based approach with such protocols, we analyzed acute myeloid leukemia (AML) bone marrow mononuclear cells measured using 10x Chromium, taken from a patient (AML035) before and after hematopoietic stem cell transplant (HSCT) (Zheng et al. 2017). Without a WES reference, we again leveraged common heterozygous variants from ExAC to identify potential heterozygous variants from pre- and post-HSCT samples. The increased number of cells enhances our ability to identify heterozygous SNPs. However, compared to the Smart-seq2, we were able to identify less than half as many SNPs in the 10x Chromium data (Supplemental Fig. 3A). Performance simulations show that with such 3'-tag data, the allele-based approach will be able to detect full chromosome and chromosome-arm level alternations but will be substantially limited in identifying more focal alterations (Supplemental Fig. 3B). While we were not able to identify any such large-scale copy-number alterations in the AML sample (Supplemental Fig. 3C, D), when examining both pre- and post-HSCT samples together, the allele-based approach clearly identified allelic patterns indicative of the presence of two distinct genotypes (Supplemental Fig. 3E). Consistent with observations from the original publication (Zheng et al. 2017), we find that cells from the post-HSCT sample were genotypically distinct from the pre-HSCT sample, reflecting

successful engraftment of donor stem cells from the HSCT treatment. Thus, an allele-based approach can distinguish cellular genotypes before and after HSCT using patterns of common natural genetic variation from 3'-tag scRNA-seq data, even without external genotype information (Kang et al. 2017).

Integration of expression data enhances power and enables identification of copy-neutral LOH

In addition to allelic imbalance, the presence of deletions, on average, also leads to diminished expression of genes within affected loci compared to copy-neutral expression references of the same cell type (Mayshar et al. 2010; Macaulay et al. 2015). Similarly, presence of amplifications, on average, leads to increased expression of genes within affected loci compared to copy-neutral expression references of the same cell type. Assessment of these expression-based karyotyping approaches has so far been qualitative in nature (Patel et al. 2014; Tirosh et al. 2016), and the extent to which they are able to capture smaller, focal deletions remains to be quantified. To provide such a quantitative evaluation, we implemented an expression-based HMM to identify regions potentially affected by CNVs as well as a Bayesian hierarchical model to assess the posterior probabilities of alterations using normalized expression data (Supplemental Fig. 4A). As before, we simulated deletions of varying size and clonality by inserting fragments of known deletions into CNV-neutral regions in MGH31 (see Methods). We find that the quantitative expression-based approach, is able to identify chromosome-arm-level clonal and nearly-clonal alterations with high sensitivity and precision (Supplemental Fig. 4C-E), but has difficulties resolving smaller, subclonal alterations as accurately as the allele-based approach. We find that the expression-based approach is particularly sensitive to the normalization reference used (Supplemental Fig. 4B). With modern scRNA-seq datasets often capturing many diverse cell types, independent normalization of different cell types by corresponding references may be necessary.

Joint consideration of both allele and expression-based evidence should increase predictive power. It should also allow distinguishing deletions from copy-neutral LOH events. We therefore extended HoneyBADGER to incorporate both types of evidence in inferring the posterior probability of affected regions identified by either the

allele or expression-based HMMs. Indeed, we find that an integrated model offers improved performance in distinguishing regions of deletion from neutral regions (Fig. 4C, Supplemental Fig. 4F). While high copy number amplifications are common in cancer, the measurements of gene expression as well as allelic imbalance are too variable to confidently infer the exact copy number. Our approach, therefore, does not infer the precise copy number, but is aimed at distinguishing deletion, amplification, and LOH regions from the unaffected regions.

To demonstrate the utility of our integrated approach, we applied HoneyBADGER to 55 breast cancer cells from patient BC09 from Chung *et al.* (Chung et al. 2017). Chung *et al.* previously identified several cells to harbor known breast cancer-related point mutations including mutations in *LRPAP1, MARCH6, ANKFY1, DNMT1, GTPBP3, BLZF1, POLA2, TMEM189, AGO3, NNT, PLK4*, and *CPSF1* (Supplemental Table 2). However, these cells were inferred to be normal based on expression-based karyotyping, suggesting a likely misclassification by the expression-based approach. Re-analysis with the allele-based model of HoneyBADGER shows that these cells harbor multiple chromosome-arm and chromosome-level abnormalities (Supplemental Fig. 4). We confirm using bulk WES (Supplemental Table 2) that such misclassification arose due to copy-neutral LOH, where copy number is maintained thus resulting in limited changes in normalized expression but detectable allelic imbalance. Our allele and expression-combined approach is thus able to identify copy-neutral LOH events and segregate tumor in a way consistent with the point mutation evidence (Supplemental Fig. 5).

To further evaluate the utility of our integrated approach with 3'-tag droplet-based scRNA-seq measurements, we applied HoneyBADGER to 1340 single cells from an unsorted bone marrow biopsy from a multiple myeloma patient (MM135) prepared using the 10x Chromium protocol. To determine the appropriate normalization for the expression data, we first applied our allele-based approach to identify a deletion on Chr 13, which separated a set of putative normal cells lacking the deletion (Supplemental Fig. 6A). We confirmed using expression-based clustering analysis that these putative normal cells did not express known MM marker genes (Supplemental Fig. 6B). Expression profiles of these putative normal cells were then averaged to serve as a normal expression reference. We then applied our integrated approach to identify a number of chromosome-arm and chromosome-

level abnormalities on Chr 1, 8, 11, 13, and 22 (Supplemental Fig. 6C-E, Supplemental Table 3). Unbiased hierarchical clustering on the posterior probabilities of these alterations effectively separated MM from non-MM cells (Supplemental Fig. 6E). We confirmed the identified chromosomal aberrations using FISH and cytogenetics (Supplemental Table 3). In addition to the chromosomal abnormalities identified by HoneyBADGER, FISH and cytogenetics identified an additional Chr 18 deletion that was missed by our computational approach due to the low number of expressed gene and detected SNPs within the region, resulting in high uncertainty. Thus, while we were able to accurately identify most chromosome-arm and chromosome-level abnormalities in this 3'-tag scRNA-seq dataset, lower SNP density in such data results in low sensitivity, as expected from previous benchmarks (Supplemental Fig. 4F).

Analysis of progressive multiple myeloma identifies genetic subclones with distinct transcriptional signatures

To examine the interaction of genetic and transcriptional heterogeneity in a context of MM progression, we applied HoneyBADGER to analyze tumor samples from a treatment-refractory MM patient (MM34), collected at two distinct time points. The initial MM sample (MM34) was collected from the bone marrow (BM) at the time of diagnosis, and a second extramedullary MM (MM34A) sample was collected from an ascites dissemination following two months of unsuccessful thalidomide/dexamethazone and bortezomib treatment.

We first applied HoneyBADGER to identify regions of CNV in 63 extramedullary MM cells from MM34A. Our allele-based HMM identified clonal deletions on multiple chromosomes including Chr 1, 2, 3, 8, 13, 16, and 17, and our expression-based HMM identified a clonal amplification on Chr 3 (Fig. 5A, Supplemental Fig. 7A, Supplemental Table 4). We confirm these CNVs by bulk WES (Supplemental Fig. 7A).

Next, we sought to identify these deletions in 65 BM MM cells from MM34 using our integrated approach. We find that while nearly all cells from MM34 harbor the Chr 13 deletion, only a fraction harbors the Chr 16, and 17 deletions, indicative of a linear subclonal expansion (Fig. 5A, Supplemental Fig. 7B). Consistent with

HoneyBADGER's findings, in the initial BM MM sample, CNV analysis from bulk WES identified a deletion on Chr 13 (Supplemental Fig. 7B), while FISH and cytogenetics analysis of 200 interphase cells also identified deletion on Chr 13 in 61% cells in addition to deletion of MAF (16q23) in 38% and p53 (17p13.1) in 11.5% cells (Supplemental Fig. 7C). The percentage of MM cells harboring each deletion inferred from HoneyBADGER was found to be consistent with the estimates from FISH and cytogenetics and bulk WES in both samples (Supplemental Fig. 7D). Based on these findings, we speculate that a genetic subclone harboring deletions on Chr 13, Chr 16, and Chr 17 most likely expanded to seed the extramedullary MM dissemination, acquiring additional alterations during this process (Fig. 5C).

Having identified this extramedullary-like subclone in the initial BM biopsy, we next examined its transcriptional signature. We identified 132 consistently differentially expressed genes (p-value < 0.05) when comparing the extramedullary-like subclone with other BM-specific MM cells in MM34 as well as jointly with the extramedullary MM cells in MM34A (Fig. 5B, Supplemental Fig. 8, Supplemental Table 5). Among the down-regulated genes, *E2F4, DPEP2,* and *CDH1* are located in the deleted region of Chr 16, indicating direct effects on gene expression from the genotype. These genes function in the suppression of cell cycle progression, activation of proinflammatory cytokines through leukotrienes, or cell adhesion events commonly suppressed during the tumor progression and metastasis (Thiery 2002; Ren et al. 2002). Among the rest of transcriptional changes, upregulation of cell cycle associated genes are likely conferred by the release of *E2F4* repressor complexes from their promoters. It is noteworthy that Chr 17 deletion preceded that of Chr 16, suggesting that downregulation of *TP53* on Chr 17 and *E2F4* has cooperated for the cell cycle progression during tumor evolution. As *CDH1* and *DPEP2* function in protein networks, the downstream effects are less visible in the transcriptional changes. Gene set enrichment analysis (GSEA) (Subramanian et al. 2005) of genes upregulated (p < 0.1) in the extramedullary-like subclone showed significant enrichment (q-value < 0.05) in the genes associated with cell cycle and a known partial response signature in MM (Zhan et al. 2006), while genes downregulated (p < 0.1) showed significant enrichment (q-value < 0.05) in immune response processes (Fabregat et al. 2016; Milacic et al. 2012) (Fig. 5D,

Supplemental Table 6). Thus, by identifying genetic subclones from scRNA-seq data, we can assess the functional impact of subclonal alterations at the transcriptional level.

Unbiased analysis of transcriptional heterogeneity identified aspects independent of the subclonal structure

Despite significant transcriptional differences between genetic subclones, alternative sources of heterogeneity, such as differences in epigenetic state or cellular microenvironment, may impact transcriptional state and ultimately phenotypic heterogeneity. Our inference of genetic information from scRNA-seq data provides a unique opportunity to assess the relative impact of these mechanisms on transcriptional state. To do so, we first characterized transcriptional heterogeneity in MM34 using pathway and gene set over-dispersion analysis (PAGODA) (Fan et al. 2016), which identifies non-redundant aspects of significant coordinated variability within annotated pathways and correlated gene sets (Fig. 6). PAGODA identified prominent aspects of transcriptional heterogeneity driven by ribosomal processes marking key transcriptional subpopulations. Other aspects of transcriptional heterogeneity were driven by expression of T-cell chemokines *CCL3* and *CCL4*, as well as *B2M* and genes involved in antigen presentation. *CCL3* and *CCL4* have been previously implicated in MM tumor growth through regulation of the MM microenvironment (Vallet et al. 2011; Roodman 2002). Likewise *B2M* has been used to predict MM progression (Rossi et al. 2010). Previously, anti-B2M monoclonal antibodies have been also shown to overcome bortezomib resistance in MM (Zhang et al. 2015), thus providing potential therapeutic implications for early discovery of these subpopulations. Surprisingly, when we compare these key transcriptional subpopulations with the inferred subclonal cell populations we find that many of the identified aspects of transcriptional heterogeneity are independent of the subclonal structure. The extramedullary-like subclone was best matched by a less prominent aspect of transcriptional heterogeneity involved in immune response. Thus, while the aspect of transcriptional heterogeneity corresponding to the genetic subclonal structure is apparent from the unbiased transcriptional analysis alone, alternative non-clonal mechanisms can drive more prominent aspects of transcriptional variation.

DISCUSSION

Altogether, our results demonstrate the ability to integrate genetic and transcriptional information using scRNA-seq data to identify and characterize transcriptional programs driving distinct genetic subclones. We show that compared to an expression-based approach, an allele-based analysis offers substantially greater sensitivity and precision in identifying deletions that are smaller on the chromosome scale, or present at lower subclonal fraction within the measured cell population. Combining allele and expression-based approaches further improves performance and enables to identification of copy-neutral LOH events. Our approach accurately recapitulates expected cancer cell fractions in single cells compared to bulk estimates, can robustly distinguish tumor from normal cells based on identified CNVs, and is suitable for both full-transcript-length and 3'-tagging scRNA-seq protocols. Examining MM patient data, we find that while key genetic subclones do exhibit distinct transcriptional signatures that likely contribute to cancer progression, other more prominent aspects of transcriptional heterogeneity can be independent of the genetic subclonal structure and are most likely driven by alternative mechanisms, including potentially variation in epigenetic state or microenvironment. By inferring genotype information from scRNA-seq data, our approach can help unravel the impact of genetic and transcriptional heterogeneity and their interplay in cancer progression.

METHODS

Patient samples and library generation

This study was approved by the institutional review board (IRB) of Samsung Medical Center (IRB approval no. SMC2013-09-009-012) and carried out in accordance with the principles of the Declaration of Helsinki. The study subjects were Korean patients diagnosed with multiple myeloma at Samsung Medical Center, Seoul, Korea. Bone marrow aspirates or ascites were subjected to Ficoll-Paque PLUS (GE Healthcare, USA) gradient and

magnetic separation with anti-CD138 antibody microbeads (Miltenyi Biotech, Germany). From the $CD138^-$ enriched cells, genomic DNA and RNA was purified using the ALLPrep kit (Qiagen, USA). Matching blood DNA was isolated by the QIAamp DNA blood kit (Qiagen). Normal control RNA was collected from $CD19^+$ microbead-purified blood B cells from four healthy volunteers. For bulk WES, genomic DNA (1 μo) from the bone marrow and matching blood samples was sheared by Covaris S220 (Covaris, MA, USA) and used for library construction with SureSelect XT Human All Exon v5 and SureSelect XT reagent kit, HSQ (Agilent Technologies, Santa Clara, CA, USA) according to manufacturer's protocols. After multiplexing, the libraries were sequenced on the HiSeq 2500 sequencing platform (Illumina, USA), using the 100 bp paired-end mode of the TruSeq Rapid PE Cluster kit and TruSeq Rapid SBS kit (Illumina). For scRNA-seq, CD138-enriched cells were subjected to single cell capture and cDNA amplification using the C1™ Single-Cell Auto Prep System (Fluidigm, South San Francisco, CA, USA) with the SMARTer kit (Clontech, Mountain View, CA, USA). Sequencing libraries were generated and multiplexed using Nextera XT DNA Sample Prep Kit (Illumina) and sequenced on the HiSeq2500 in the 100-bp paired-end mode of the TruSeq Rapid PE Cluster kit and TruSeq Rapid SBS kit following the Smart-seq2 protocol (Picelli et al. 2014).

Bulk WES analysis

Reads from the FASTQ files were mapped against the human reference genome (GRCh37) using BWA MEM v0.7.8 (Li and Durbin 2010). Duplicates were removed using Picard tools v1.87 (https://broadinstitute.github.io/picard/). Indel realignment and quality score recalibration was performed using GATK v3.3.0 based on the GATK best practices guidelines (DePristo et al. 2011). Germline heterozygous variants were then identified using GATK's UnifiedGenotyper followed by variant quality score recalibration. To identify copy number alterations, mapped BAMs were analyzed by FREEC v7.2 with parameters recommended for WES data analysis by the authors (coefficientOfVariation = 0.062, window = 500, step = 250, breakPointThreshold = 1.5, readCountThreshold = 50, noisyData = TRUE) (Boeva et al. 2011). Genomic coordinates for copy number alternation were identified from the outputted text summaries and used for downstream analysis. To estimate subclonal deletion frequencies from bulk WES, the following equation was

used based on an assumption of 100% purity: $b = f * 0 + (1 - f) * 0.5$, where b is the average LAF (lesser allele fraction), and f is subclonal fraction for deletion. This leads to: $f = 1 - 2b$. The LAF value of a deletion region was obtained by averaging LAF values over the segments within the region. The segments and their LAF values were determined by FREEC.

Evaluating SNP detection rates from bulk and single-cell RNA-seq data

Single-nucleotide variants were called on bulk and single-cell K562 paired-end RNA-seq data using TopHat2 (Kim et al. 2013) and Genome Analysis Toolkit (GATK) (McKenna et al. 2010; DePristo et al. 2011). Bulk K562 data (Deng et al. 2011) was downloaded from Short Read Archive (accession SRR315337) using SRAToolkit v2.5.7. Single-cell K562 RNA-seq measurements were carried out using C1™ Single-Cell Auto Prep System, in the same way as MM cells. Variants were called separately on the individual cell (instead of joint calling) for a fair comparison to bulk data, which was also separately fed to the same variant calling pipeline. Later, to match precision, single-cell variants that occurred in only one cell were discarded. Alignment was performed using TopHat v2.0.10 (along with Bowtie 2 v2.1.0 (Langmead and Salzberg 2012)) against human genome v37 with decoy, allowing two mismatches and two gaps and the --max-multihits=2 option to report up to two alignments per read. Then, only uniquely aligned reads were kept. Human GRCh37.73 transcriptome annotation was used to guide spliced mapping. Aligned reads were sorted by coordinates using SAMtools v0.1.19 (Li et al. 2009) and duplicates were removed using Picard v1.107 (https://broadinstitute.github.io/picard/) MarkDuplicates. GATK 3.0.0 was used for the subsequent processing, including Indel Realignment, Base Quality Score Recalibration (BQSR), Unified Genotyper and Variant Quality Score Recalibration (VQSR). The -U ALLOW_N_CIGAR_READS option was used to handle spliced reads. To provide known polymorphic sites to GATK, dbSNP 138 was used for single-nucleotide substitutions and Mills_and_1000G_gold_standard.indels for known indel sites. After VQSR, only variants marked as 'PASS' were kept. Likewise, for previously published scRNA-seq data from Patel et al., SRA files were downloaded from GEO (accession GSE57872) and converted to FASTQs using SRAToolKit v2.3.5. Alignment was performed using TopHat2 v2.0.10 (along with Bowtie 2 v2.1.048) against human genome v37 with decoy, allowing two mismatches and two gaps and the --max-

multihits=2 option to report up to two alignments per read. Then, only uniquely aligned reads were kept. Human GRCh37.73 transcriptome annotation was used to guide spliced mapping. Aligned reads were sorted by coordinates using SAMtools v0.1.1949 and duplicates were removed using Picard v1.107 (https://broadinstitute.github.io/picard/) MarkDuplicates.

Heterozygous SNP identification

Where bulk WES data is available, heterozygous SNPs were called directly from bulk WES using GATK 3.0.0. Where bulk WES was not available, common heterozygous variants were identified from the Exome Aggregation Consortium (ExAC) variant sites database. ExAC variants were filtered to include single nucleotide variants only with minor allele frequency > 10%. Variants were further filtered based on presence within the dataset of interest. Variants were considered heterozygous if reads from both the annotated reference and alternate alleles were present and distributed according to $Bin(p = 0.5, n) > 1x10^{-8}$, where n is the total read coverage at that SNP. Resulting putative heterozygous SNPs were used to generate allele count matrices to assess the reference and alternative allele counts at each position using Rsamtools v1.28.0 (Morgan et al. 2018).

Single-cell analysis

For gene expression quantification, reads from the FASTQ files were mapped against the USCS hg19 human reference genome using TopHat2 v2.1.0 (Kim et al. 2013) and quantified using featureCounts v1.4.4 (Liao et al. 2014). We do not anticipate realigning reads to GRCh38 will affect conclusions as coding SNPs relevant to our analysis remain largely consistent between the two builds. For the previously published single-cell RNA-seq data from Patel *et al.*, expression matrices were downloaded from GEO (accession GSE57872). Differential expression analysis on the two identified subclones was performed using SCDE (v1.99.1) (Kharchenko et al. 2014; Fan et al. 2016) with default parameters following recommended protocols (http://hms-dbmi.github.io/scde/diffexp.html). Significantly differentially expressed genes were identified using an absolute non-corrected Z-score cut-off of 1.96, corresponding to p-value < 0.05, for heatmap visualization, and 1.28, corresponding to p-value < 0.2, for gene set enrichment analysis. Gene set enrichment analysis was performed using the LIGER

(https://github.com/JEFworks/liger) package with input values as sorted MLE estimates of fold-change limited to significantly differentially expressed genes. In total, 10593 curated (C2), GO (C5), oncogenic (C6), and immune (C7) gene sets from MSigDB (Liberzon et al. 2015) were tested. Gene sets with less than 5 genes or more than 500 genes were omitted. Pathway and geneset overdispersion analysis to identify transcriptional subpopulations was performed using PAGODA (SCDE v1.99.1) (Fan et al. 2016; Kharchenko et al. 2014) with the same gene sets.

Hidden Markov model

HoneyBADGER implements an expression-based HMM as well as an allele-based HMM to identify regions potentially affected by CNVs. For the expression-based HMM, a transition matrix is defined on 3 hidden states representing deletion, neutral, and amplification $\begin{bmatrix} 1-2t & t & t \\ t & 1-2t & t \\ t & t & 1-2t \end{bmatrix}$ where t=1e-5 by default. Emission probabilities are defined by a normal distribution with means and variance estimated from the normalized expression data (see *Expression-based approach*). For the allele-based HMM, a transition matrix is defined on 2 hidden states representing deletion or LOH, and neutral $\begin{bmatrix} 1-t & t \\ t & 1-t \end{bmatrix}$ where t=1e-5 by default. Emission probabilities are defined by a binomial distribution with the size parameter given by the pooled coverage at the SNP position and an expected p=0.1 for the lesser allele in the case of deletion or LOH and p=0.45 for neutral. Default transition probabilities transition have been set based on the size of the regions expected to be able to detect. We find that both the expression-based HMM and allele-based HMM is robust to choices of transition probability t (Supplemental Fig. 9). However, for genomic regions and protocols with high rates of erroneous SNP detection or high normalized expression variance due to technical noise, we anticipate that these transition probabilities may need to be tuned.

Hierarchical Bayesian model

HoneyBADGER contains implementations of an expression-based approach, an allele-based approach, ad an integrative approach for assessing the posterior probability of CNVs in given regions. All Bayesian hierarchical models were written in BUGs for Gibbs sampling. Simulation from the models using MCMC was accomplished through rJAGS. Four chains were initialized specifying starting values for S^k and dd^k as 0 or 1 in all possible permutations where appropriate. The MCMC chains were allowed to run for 1000 iterations, with an adaptation of 100 and a burn-in of 100. Trace plots were used to ensure appropriate mixing on the hyper parameters and Gelman plots were used to diagnose convergence of chains (Supplemental Fig. 10A, B).

For a particular region of interest, our goal is to make inference on the copy number status of a cell for that region given its observed allelic imbalance for germline heterozygous SNPs within the region and gene expression in the region relative to a putative diploid expression reference of comparable cell type. For a candidate region, let $S^k = 1$ if cell k has a copy number variation and $S^k = 0$ if cell k is copy number neutral.

In both allele and expression-based models, we seek to estimate the posterior distribution of S^k given the observations. We can accomplish this through a hierarchical Bayesian framework, modeling the observed gene expression as a function of the variables of interest $\left[S^k, dd^k \mid \overline{gexp^k} \right] \propto \left[\overline{gexp^k} \mid S^k, dd^k \right][S^k, dd^k] = \left[\overline{gexp^k} \mid S^k, dd^k \right][S^k][dd^k]$ where $dd^k = 1$ for a copy number gain and $dd^k = 0$ for a copy number loss, such that S^k and dd^k together capture the copy number status for cell k, and $\overline{gexp^k}$ is the observed average normalized gene expression for genes within the tested region of interest in cell k. Likewise, for the allele-based model, we model observations at both the individual cell and bulk or pooled SNP-level information integrated into an additional hierarchical level involving observed gene-level mono-allelic expression rates. An additional combined model approach makes inference on S^k using both gene expression and allele information.

Data access

The scRNA-seq and WES data for the MM cells have been submitted to the NCBI Gene Expression Omnibus (GEO; http://www.ncbi.nlm.nih.gov/geo/) under accession number GSE110499. HoneyBADGER is freely available under the GPL and is available as an R package (R Core Team 2017) with the source code available in

the Supplementary Material and on GitHub (https://github.com/JEFworks/HoneyBADGER). Additional tutorials and documentation are available at http://jef.works/HoneyBADGER/.

ACKNOWLEDGEMENTS

JF was supported by an NIH grant F99 CA222750-01. PVK was supported by NIH R01HL131768 from NHLBI and CAREER (NSF-14-532) award from NSF. HL was supported by Korea Basic Science Research Program grant NRF-2017R1D1A1B03032194. WYP was supported by Korea Health Technology R&D project HI13C2096 through KHIDI, Ministry of Health & Welfare, Korea. We thank Patrik Ernfors for helpful feedback on the manuscript.

REFERENCES

Boeva V, Popova T, Bleakley K, Chiche P, Cappo J, Schleiermacher G, Janoueix-Lerosey I, Delattre O, Barillot E. 2012. Control-FREEC: a tool for assessing copy number and allelic content using next-generation sequencing data. *Bioinformatics* **28**: 423–5. http://www.ncbi.nlm.nih.gov/pubmed/22155870 (Accessed August 17, 2016).

Boeva V, Zinovyev A, Bleakley K, Vert J-P, Janoueix-Lerosey I, Delattre O, Barillot E. 2011. Control-free calling of copy number alterations in deep-sequencing data using GC-content normalization. *Bioinformatics* **27**: 268–9. http://www.ncbi.nlm.nih.gov/pubmed/21081509 (Accessed August 18, 2016).

Borel C, Ferreira PG, Santoni F, Delaneau O, Fort A, Popadin KY, Garieri M, Falconnet E, Ribaux P, Guipponi M, et al. 2015. Biased allelic expression in human primary fibroblast single cells. *Am J Hum Genet* **96**: 70–80. http://dx.doi.org/10.1016/j.ajhg.2014.12.001.

Chen M, Gunel M, Zhao H. 2013. SomatiCA: identifying, characterizing and quantifying somatic copy number aberrations from cancer genome sequencing data. *PLoS One* **8**: e78143.

http://www.ncbi.nlm.nih.gov/pubmed/24265680 (Accessed August 17, 2016).

Chung W, Eum HH, Lee H-O, Lee K-M, Lee H-B, Kim K-T, Ryu HS, Kim S, Lee JE, Park YH, et al. 2017. Single-cell RNA-seq enables comprehensive tumour and immune cell profiling in primary breast cancer. *Nat Commun* **8**: 15081. http://www.nature.com/doifinder/10.1038/ncomms15081 (Accessed May 23, 2017).

Deng Q, Ramsköld D, Reinius B, Sandberg R. 2014. Single-cell RNA-seq reveals dynamic, random monoallelic gene expression in mammalian cells. *Science* **343**: 193–6. http://www.ncbi.nlm.nih.gov/pubmed/24408435 (Accessed September 7, 2016).

Deng X, Hiatt JB, Nguyen DK, Ercan S, Sturgill D, Hillier LW, Schlesinger F, Davis CA, Reinke VJ, Gingeras TR, et al. 2011. Evidence for compensatory upregulation of expressed X-linked genes in mammals, Caenorhabditis elegans and Drosophila melanogaster. *Nat Genet* **43**: 1179–85. http://www.ncbi.nlm.nih.gov/pubmed/22019781 (Accessed September 7, 2016).

DePristo MA, Banks E, Poplin R, Garimella K V, Maguire JR, Hartl C, Philippakis AA, del Angel G, Rivas MA, Hanna M, et al. 2011. A framework for variation discovery and genotyping using next-generation DNA sequencing data. *Nat Genet* **43**: 491–8. http://www.ncbi.nlm.nih.gov/pubmed/21478889 (Accessed August 18, 2016).

Dey SS, Kester L, Spanjaard B, Bienko M, van Oudenaarden A. 2015. Integrated genome and transcriptome sequencing of the same cell. *Nat Biotechnol* **33**: 285–9. http://www.ncbi.nlm.nih.gov/pubmed/25599178 (Accessed August 17, 2016).

Ding L, Ley TJ, Larson DE, Miller CA, Koboldt DC, Welch JS, Ritchey JK, Young MA, Lamprecht T, McLellan MD, et al. 2012. Clonal evolution in relapsed acute myeloid leukaemia revealed by whole-genome sequencing. *Nature* **481**: 506–510.

Fabregat A, Sidiropoulos K, Garapati P, Gillespie M, Hausmann K, Haw R, Jassal B, Jupe S, Korninger F, McKay S, et al. 2016. The Reactome pathway Knowledgebase. *Nucleic Acids Res* **44**: D481-7. http://www.ncbi.nlm.nih.gov/pubmed/26656494 (Accessed September 7, 2016).

Fan J, Salathia N, Liu R, Kaeser GE, Yung YC, Herman JL, Kaper F, Fan J-B, Zhang K, Chun J, et al. 2016. Characterizing transcriptional heterogeneity through pathway and gene set overdispersion analysis. *Nat*

Methods **13**: 241–4. http://www.ncbi.nlm.nih.gov/pubmed/26780092 (Accessed August 17, 2016).

Gerlinger M, Rowan AJ, Horswell S, Larkin J, Endesfelder D, Gronroos E, Martinez P, Matthews N, Stewart A, Tarpey P, et al. 2012. Intratumor Heterogeneity and Branched Evolution Revealed by Multiregion Sequencing. *N Engl J Med* **366**: 883–892. http://www.nejm.org/doi/abs/10.1056/NEJMoa1113205 (Accessed January 25, 2017).

Glitza IC, Lu G, Shah R, Bashir Q, Shah N, Champlin RE, Shah J, Orlowski RZ, Qazilbash MH. 2015. Chromosome 8q24.1/c-MYC abnormality: a marker for high-risk myeloma. *Leuk Lymphoma* **56**: 602–7. http://www.ncbi.nlm.nih.gov/pubmed/24844357 (Accessed August 17, 2016).

Kang HM, Subramaniam M, Targ S, Nguyen M, Maliskova L, McCarthy E, Wan E, Wong S, Byrnes L, Lanata CM, et al. 2017. Multiplexed droplet single-cell RNA-sequencing using natural genetic variation. *Nat Biotechnol*. http://www.nature.com/doifinder/10.1038/nbt.4042 (Accessed December 20, 2017).

Kharchenko P V, Silberstein L, Scadden DT. 2014. Bayesian approach to single-cell differential expression analysis. *Nat Methods* **11**: 740–2. http://www.ncbi.nlm.nih.gov/pubmed/24836921.

Kim D, Pertea G, Trapnell C, Pimentel H, Kelley R, Salzberg SL. 2013. TopHat2: accurate alignment of transcriptomes in the presence of insertions, deletions and gene fusions. *Genome Biol* **14**: R36. http://www.ncbi.nlm.nih.gov/pubmed/23618408 (Accessed August 18, 2016).

Klein AM, Mazutis L, Akartuna I, Tallapragada N, Veres A, Li V, Peshkin L, Weitz DA, Kirschner MW. 2015. Droplet Barcoding for Single-Cell Transcriptomics Applied to Embryonic Stem Cells. *Cell* **161**: 1187–1201. http://www.sciencedirect.com/science/article/pii/S0092867415005000.

Langmead B, Salzberg SL. 2012. Fast gapped-read alignment with Bowtie 2. *Nat Methods* **9**: 357–9. http://www.ncbi.nlm.nih.gov/pubmed/22388286 (Accessed September 7, 2016).

Lek M, Karczewski KJ, Minikel E V., Samocha KE, Banks E, Fennell T, O'Donnell-Luria AH, Ware JS, Hill AJ, Cummings BB, et al. 2016. Analysis of protein-coding genetic variation in 60,706 humans. *Nature* **536**: 285–291. http://www.nature.com/doifinder/10.1038/nature19057 (Accessed December 20, 2017).

Li H, Durbin R. 2010. Fast and accurate long-read alignment with Burrows-Wheeler transform. *Bioinformatics* **26**: 589–95. http://www.ncbi.nlm.nih.gov/pubmed/20080505 (Accessed August 18, 2016).

Li H, Handsaker B, Wysoker A, Fennell T, Ruan J, Homer N, Marth G, Abecasis G, Durbin R, 1000 Genome Project Data Processing Subgroup. 2009. The Sequence Alignment/Map format and SAMtools. *Bioinformatics* **25**: 2078–9. http://www.ncbi.nlm.nih.gov/pubmed/19505943 (Accessed September 7, 2016).

Liao Y, Smyth GK, Shi W. 2014. featureCounts: an efficient general purpose program for assigning sequence reads to genomic features. *Bioinformatics* **30**: 923–30. http://www.ncbi.nlm.nih.gov/pubmed/24227677 (Accessed August 18, 2016).

Liberzon A, Birger C, Thorvaldsdóttir H, Ghandi M, Mesirov JP, Tamayo P. 2015. The Molecular Signatures Database (MSigDB) hallmark gene set collection. *Cell Syst* **1**: 417–425. http://www.ncbi.nlm.nih.gov/pubmed/26771021 (Accessed August 17, 2016).

Lohr J, Stojanov P, Carter S, Cruz-Gordillo P, Lawrence M, Auclair D, Sougnez C, Knoechel B, Gould J, Saksena G, et al. 2014. Widespread genetic heterogeneity in multiple myeloma: Implications for targeted therapy. *Cancer Cell* **25**: 91–101.

Macaulay IC, Haerty W, Kumar P, Li YI, Hu TX, Teng MJ, Goolam M, Saurat N, Coupland P, Shirley LM, et al. 2015. G&T-seq: parallel sequencing of single-cell genomes and transcriptomes. *Nat Methods* **12**: 519–22. http://www.ncbi.nlm.nih.gov/pubmed/25915121 (Accessed August 17, 2016).

Macosko EZ, Basu A, Satija R, Nemesh J, Shekhar K, Goldman M, Tirosh I, Bialas AR, Kamitaki N, Martersteck EM, et al. 2015. Highly Parallel Genome-wide Expression Profiling of Individual Cells Using Nanoliter Droplets. *Cell* **161**: 1202–1214. http://www.ncbi.nlm.nih.gov/pubmed/26000488 (Accessed November 30, 2017).

Mayshar Y, Ben-David U, Lavon N, Biancotti J-C, Yakir B, Clark AT, Plath K, Lowry WE, Benvenisty N. 2010. Identification and classification of chromosomal aberrations in human induced pluripotent stem cells. *Cell Stem Cell* **7**: 521–31. http://www.ncbi.nlm.nih.gov/pubmed/20887957 (Accessed August 17, 2016).

McKenna A, Hanna M, Banks E, Sivachenko A, Cibulskis K, Kernytsky A, Garimella K, Altshuler D, Gabriel S, Daly M, et al. 2010. The Genome Analysis Toolkit: a MapReduce framework for analyzing next-generation DNA sequencing data. *Genome Res* **20**: 1297–303. http://www.ncbi.nlm.nih.gov/pubmed/20644199 (Accessed September 7, 2016).

Melchor L, Brioli A, Wardell CP, Murison A, Potter NE, Kaiser MF, Fryer RA, Johnson DC, Begum DB, Hulkki Wilson S, et al. 2014. Single-cell genetic analysis reveals the composition of initiating clones and phylogenetic patterns of branching and parallel evolution in myeloma. *Leukemia* **28**: 1705–15. http://www.ncbi.nlm.nih.gov/pubmed/24480973 (Accessed August 17, 2016).

Milacic M, Haw R, Rothfels K, Wu G, Croft D, Hermjakob H, D'Eustachio P, Stein L. 2012. Annotating cancer variants and anti-cancer therapeutics in reactome. *Cancers (Basel)* **4**: 1180–211. http://www.ncbi.nlm.nih.gov/pubmed/24213504 (Accessed September 7, 2016).

Morgan M, Pagès H, Obenchain V, Hayden N. 2018. Rsamtools: Binary alignment (BAM), FASTA, variant call (BCF), and tabix file import. http://bioconductor.org/packages/release/bioc/html/Rsamtools.html.

Mroz EA, Tward AM, Hammon RJ, Ren Y, Rocco JW. 2015. Intra-tumor Genetic Heterogeneity and Mortality in Head and Neck Cancer: Analysis of Data from The Cancer Genome Atlas. *PLoS Med* **12**: e1001786. http://journals.plos.org/plosmedicine/article?id=10.1371/journal.pmed.1001786 (Accessed February 11, 2015).

Patel AP, Tirosh I, Trombetta JJ, Shalek AK, Gillespie SM, Wakimoto H, Cahill DP, Nahed B V, Curry WT, Martuza RL, et al. 2014. Single-cell RNA-seq highlights intratumoral heterogeneity in primary glioblastoma. *Science* **344**: 1396–401. http://www.ncbi.nlm.nih.gov/pubmed/24925914 (Accessed July 9, 2014).

Picelli S, Faridani OR, Björklund ÅK, Winberg G, Sagasser S, Sandberg R. 2014. Full-length RNA-seq from single cells using Smart-seq2. *Nat Protoc* **9**: 171–181. http://www.nature.com/doifinder/10.1038/nprot.2014.006 (Accessed March 24, 2018).

R Core Team. 2017. R: A Language and Environment for Statistical Computing. https://www.r-project.org.

Ren B, Cam H, Takahashi Y, Volkert T, Terragni J, Young RA, Dynlacht BD. 2002. E2F integrates cell cycle progression with DNA repair, replication, and G2/M checkpoints. *Genes Dev* **16**: 245–256. http://www.ncbi.nlm.nih.gov/pubmed/11799067 (Accessed June 29, 2017).

Roodman GD. 2002. Role of the bone marrow microenvironment in multiple myeloma. *J Bone Miner Res* **17**: 1921–5. http://www.ncbi.nlm.nih.gov/pubmed/12412796 (Accessed August 17, 2016).

Rossi D, Fangazio M, De Paoli L, Puma A, Riccomagno P, Pinto V, Zigrossi P, Ramponi A, Monga G, Gaidano G. 2010. Beta-2-microglobulin is an independent predictor of progression in asymptomatic multiple myeloma. *Cancer* **116**: 2188–200. http://www.ncbi.nlm.nih.gov/pubmed/20198709 (Accessed August 17, 2016).

Sekiguchi N, Ootsubo K, Wagatsuma M, Midorikawa K, Nagata A, Noto S, Yamada K, Takezako N. 2014. Impact of C-Myc gene-related aberrations in newly diagnosed myeloma with bortezomib/dexamethasone therapy. *Int J Hematol* **99**: 288–95. http://www.ncbi.nlm.nih.gov/pubmed/24496825 (Accessed August 17, 2016).

Shah SP, Roth A, Goya R, Oloumi A, Ha G, Zhao Y, Turashvili G, Ding J, Tse K, Haffari G, et al. 2012. The clonal and mutational evolution spectrum of primary triple-negative breast cancers. *Nature* **486**: 395. http://www.nature.com/doifinder/10.1038/nature10933 (Accessed January 25, 2017).

Subramanian A, Tamayo P, Mootha VK, Mukherjee S, Ebert BL, Gillette MA, Paulovich A, Pomeroy SL, Golub TR, Lander ES, et al. 2005. Gene set enrichment analysis: a knowledge-based approach for interpreting genome-wide expression profiles. *Proc Natl Acad Sci U S A* **102**: 15545–50. http://www.ncbi.nlm.nih.gov/pubmed/16199517 (Accessed August 17, 2016).

Thiery JP. 2002. Epithelial–mesenchymal transitions in tumour progression. *Nat Rev Cancer* **2**: 442–454. http://www.ncbi.nlm.nih.gov/pubmed/12189386 (Accessed July 18, 2017).

Tirosh I, Izar B, Prakadan SM, Wadsworth MH, Treacy D, Trombetta JJ, Rotem A, Rodman C, Lian C, Murphy G, et al. 2016. Dissecting the multicellular ecosystem of metastatic melanoma by single-cell RNA-seq. *Science* **352**: 189–96. http://www.ncbi.nlm.nih.gov/pubmed/27124452 (Accessed August 17, 2016).

Vallet S, Pozzi S, Patel K, Vaghela N, Fulciniti MT, Veiby P, Hideshima T, Santo L, Cirstea D, Scadden DT, et al. 2011. A novel role for CCL3 (MIP-1α) in myeloma-induced bone disease via osteocalcin downregulation and inhibition of osteoblast function. *Leukemia* **25**: 1174–81. http://www.ncbi.nlm.nih.gov/pubmed/21403648 (Accessed August 17, 2016).

Vogelstein B, Papadopoulos N, Velculescu VE, Zhou S, Diaz LA, Kinzler KW. 2013. Cancer genome landscapes. *Science* **339**: 1546–58. http://www.ncbi.nlm.nih.gov/pubmed/23539594 (Accessed August 17, 2016).

Walker BA, Wardell CP, Melchor L, Brioli A, Johnson DC, Kaiser MF, Mirabella F, Lopez-Corral L, Humphray S, Murray L, et al. 2014. Intraclonal heterogeneity is a critical early event in the development of myeloma and precedes the development of clinical symptoms. *Leukemia* **28**: 384–90. http://www.ncbi.nlm.nih.gov/pubmed/23817176 (Accessed August 17, 2016).

Wang K, Li M, Hadley D, Liu R, Glessner J, Grant SFA, Hakonarson H, Bucan M. 2007. PennCNV: an integrated hidden Markov model designed for high-resolution copy number variation detection in whole-genome SNP genotyping data. *Genome Res* **17**: 1665–74. http://www.ncbi.nlm.nih.gov/pubmed/17921354 (Accessed August 17, 2016).

Wang L, Fan J, Francis JM, Georghiou G, Hergert S, Li S, Gambe R, Zhou CW, Yang C, Xiao S, et al. 2017. Integrated single-cell genetic and transcriptional analysis suggests novel drivers of chronic lymphocytic leukemia. *Genome Res*. http://www.ncbi.nlm.nih.gov/pubmed/28679620 (Accessed July 18, 2017).

Wu CJ. 2012. CLL clonal heterogeneity: an ecology of competing subpopulations. *Blood* **120**.

Zhan F, Huang Y, Colla S, Stewart JP, Hanamura I, Gupta S, Epstein J, Yaccoby S, Sawyer J, Burington B, et al. 2006. The molecular classification of multiple myeloma. *Blood* **108**: 2020–8. http://www.ncbi.nlm.nih.gov/pubmed/16728703 (Accessed August 17, 2016).

Zhang M, He J, Liu Z, Lu Y, Zheng Y, Li H, Xu J, Liu H, Qian J, Orlowski RZ, et al. 2015. Anti-β_2-microglobulin monoclonal antibodies overcome bortezomib resistance in multiple myeloma by inhibiting autophagy. *Oncotarget* **6**: 8567–78. http://www.ncbi.nlm.nih.gov/pubmed/25895124 (Accessed August 17, 2016).

Zheng GXY, Terry JM, Belgrader P, Ryvkin P, Bent ZW, Wilson R, Ziraldo SB, Wheeler TD, McDermott GP, Zhu J, et al. 2017. Massively parallel digital transcriptional profiling of single cells. *Nat Commun* **8**: 14049. http://www.nature.com/doifinder/10.1038/ncomms14049 (Accessed December 20, 2017).

FIGURE LEGENDS

Figure 1. Prevalence of mono-allelic detection and sparse signals in scRNA-seq data. A) Sensitivity of heterozygous SNP detection as a function of coverage in single-cell and bulk RNA-seq data for the K562 cell line. Sensitivity was calculated as the proportion of sites that are called heterozygous in the RNA-seq sample among the sites that were called heterozygous in the WES data. Error bars show standard deviation. The coverage distribution (bottom) is shown for bulk and an average of the individual cells. **B)** Prevalence of mono-allelic detection in scRNA-seq data. Lowly expressed genes are nearly exclusively detected in a mono-allelic manner. The mono-allelic detection rate generally goes down with expression magnitude, however remains high even for well-covered polymorphisms. Error bars show the 95% confidence interval of the binomial proportions. **C)** Lesser allele fraction profile visualizes patterns of allelic imbalance for germline heterozygous SNPs identified from scRNA-seq. The dot plot illustrates coverage (size) and allele bias (color) for germline heterozygous SNPs (rows) detected in different cells (columns). The bottom row designates genes with alternating color labels. Single cells commonly exhibit stretches of mono-allelic detection within genes, as noted by the same color dots. However, across genes in a single cell, both alleles can be observed, suggesting that both alleles are present. In contrast, within a deletion region (right), single cells can only express from the non-deleted allele.

Figure 2. Overview of HoneyBADGER. CNVs and LOHs are identified from scRNA-seq data in the following 7 steps. (1) Cells are first clustered on smoothed lesser-allele frequencies. (2) Cells are split into 2 main groups and pooled (3) A hidden Markov model on the pooled lesser-allele fraction identified regions with potential CNVs or LOHs (4) A Bayesian hierarchical model assessed the posterior probability of a CNV or LOH for each region in each cell (5) Cells are clustered by their posterior probabilities of CNV or LOH for each region (6) Cells are split into putative subclones (7) Approach is recursively applied to each subclone until no new subclones can be detected.

Figure 3. HoneyBADGER analysis of 44 multiple myeloma cells. A) Lesser allele profiles where each column is a heterozygous SNP and each row is a single cell. Points are colored by the lesser allele fraction with yellow suggesting equal detection of both alleles and red and blue indicated mono-allelic detection in either direction. Points are sized by coverage at the SNP site in the given cell. Cells are ordered based on row dendrogram in C. **B)** Allele profiles for regions identified by HoneyBADGER as potential CNV or LOH regions. Width corresponds to size of region. Cells are ordered based on row dendrogram in C. **C)** Heatmap of posterior probability of CNVs or LOHs in each identified region where each column is a region and each row is a cell. Row side colors annotate cells as originating from MM16 or MM16R, and classified as Normal or Tumor. **D)** Interphase FISH and cytogenetics of cells from MM16. Of the 200 cells analyzed, 82.5% had a single D17Z1 and p53 signal, and 79.5% a single MAFB (20q12) signal. The sample analyzed is estimated to have 81-95% tumor purity by $CD138^{+}$. Representative cells shown. **E)** Copy number inference by bulk WES for MM16.

Figure 4. HoneyBADGER performance as a function of clonality and CNV size. A) Allele-model sensitivity for identifying SNPs affected by deletion. **B)** Allele-model precision for distinguishing tumor - cells with deletion - from normal - cells without. **C)** Prediction performance of HoneyBADGER's posterior probability estimates as a function of deletion size. Four different HoneyBADGER models are shown using different colors: expression-only model with PBMC and $CD19^{+}$ expression normalization reference (green); expression-only model with normal blood GTEx expression normalization reference (blue); expression and SNP combined model (purple); SNP-only model (red). Inner quartile range is indicated by the vertical lines. Performance was quantified by ROC AUC. Inset shows representative ROC curves for a simulated 25Mb deletion.

Figure 5. Transcriptional characterization of MM34 and MM34A. A) Posterior probability of alterations in MM34 and MM34A. **B)** Heatmap of 120 consistently significantly differentially expressed genes in comparing the BM-like MM cells vs. extramedullary-like MM cells in MM34, and BM-like MM cells vs. extramedullary-like MM cells in MM34 and MM34A (Supplemental Table 4). Select genes of relevance to MM or cancer based on literature search are annotated. **C)** Proposed linear pattern of subclonal evolution. **D)** Gene set enrichment

analysis shows enrichment in cell cycle processes (left) and a known MM partial response signature (middle) for genes upregulated in the extramedullary-like MM34 subclone. Whereas enrichment in immune response processes is seen for genes upregulated in the BM-like MM34 subclone.

Figure 6. Pathway and geneset overdispersion analysis of MM34. Unbiased transcriptional analysis of the initial BM biopsy sample (MM34). Hierarchical clustering of cells (columns) is shown based on their overall transcriptional similarity. Top 5 most significant (p-value < 0.05) aspects of transcriptional heterogeneity (rows) are shown by the green-orange heatmap in the center. Expression patterns of subsets of genes underlying each identified aspect of transcriptional heterogeneity are shown in the blue-red heatmaps below. Top panels show posterior probabilities of different deletions, and the consensus similarity to the extramedullary dissemination for each cell. Correspondence of different transcriptional subpopulations to the underlying subclonal structure is shown by the association heatmap (right, black-red). In particular, strong correspondence is observed between genetic subclones and the immune response aspect of transcriptional heterogeneity. However other, more prominent transcriptional subpopulations (*CCL3/CCL4*, antigen presentation) appear independently of the subclonal structure.

Fig. 1

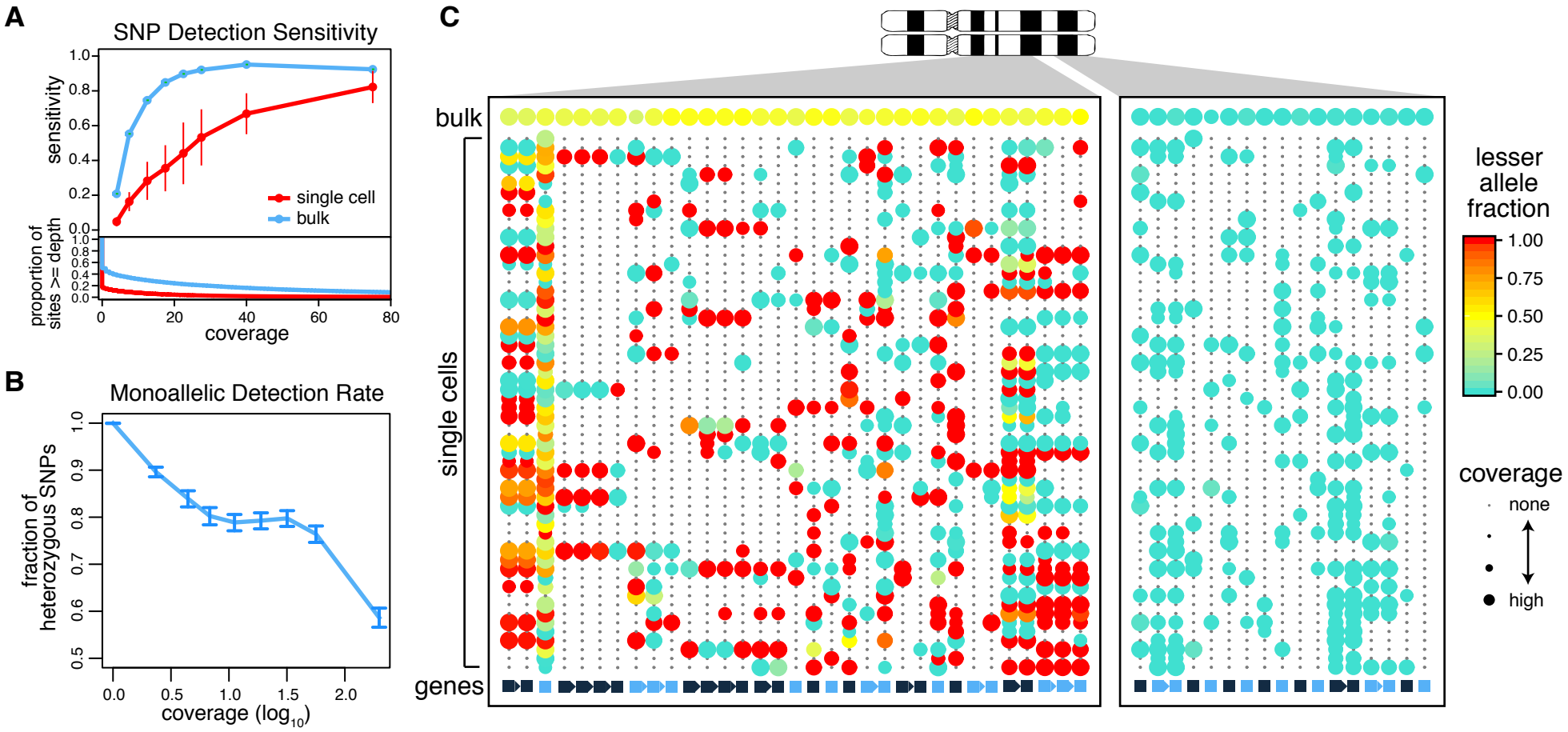
A
SNP Detection Sensitivity
sensitivity
single cell
bulk
proportion of sites >= depth
coverage
B
Monoallelic Detection Rate
fraction of heterozygous SNPs
coverage (log10)
C
bulk
single cells
genes
lesser allele fraction
1.00
0.75
0.50
0.25
0.00
coverage
none
high

Fig. 2

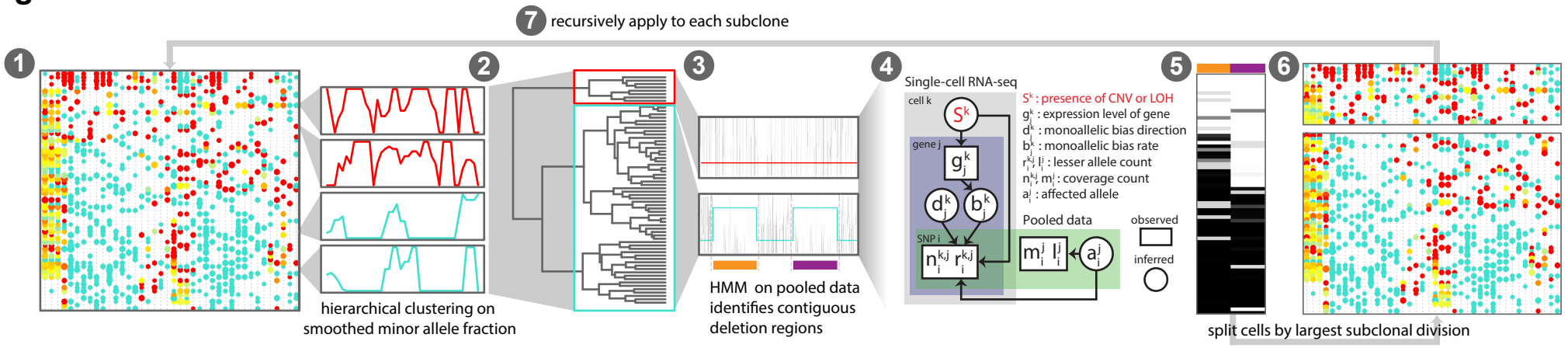
7 recursively apply to each subclone
1
2
3
4
5
6
hierarchical clustering on
smoothed minor allele fraction
HMM on pooled data
identifies contiguous
deletion regions
Single-cell RNA-seq
cell k
gene j
SNP i
Pooled data
observed
inferred
S^k : presence of CNV or LOH
g_j^k : expression level of gene
d_j^k : monoallelic bias direction
b_j^k : monoallelic bias rate
$r_i^{k,j}, l_i^j$: lesser allele count
$n_i^{k,j}, m_i^j$: coverage count
a_i^j : affected allele
split cells by largest subclonal division

Fig. 3

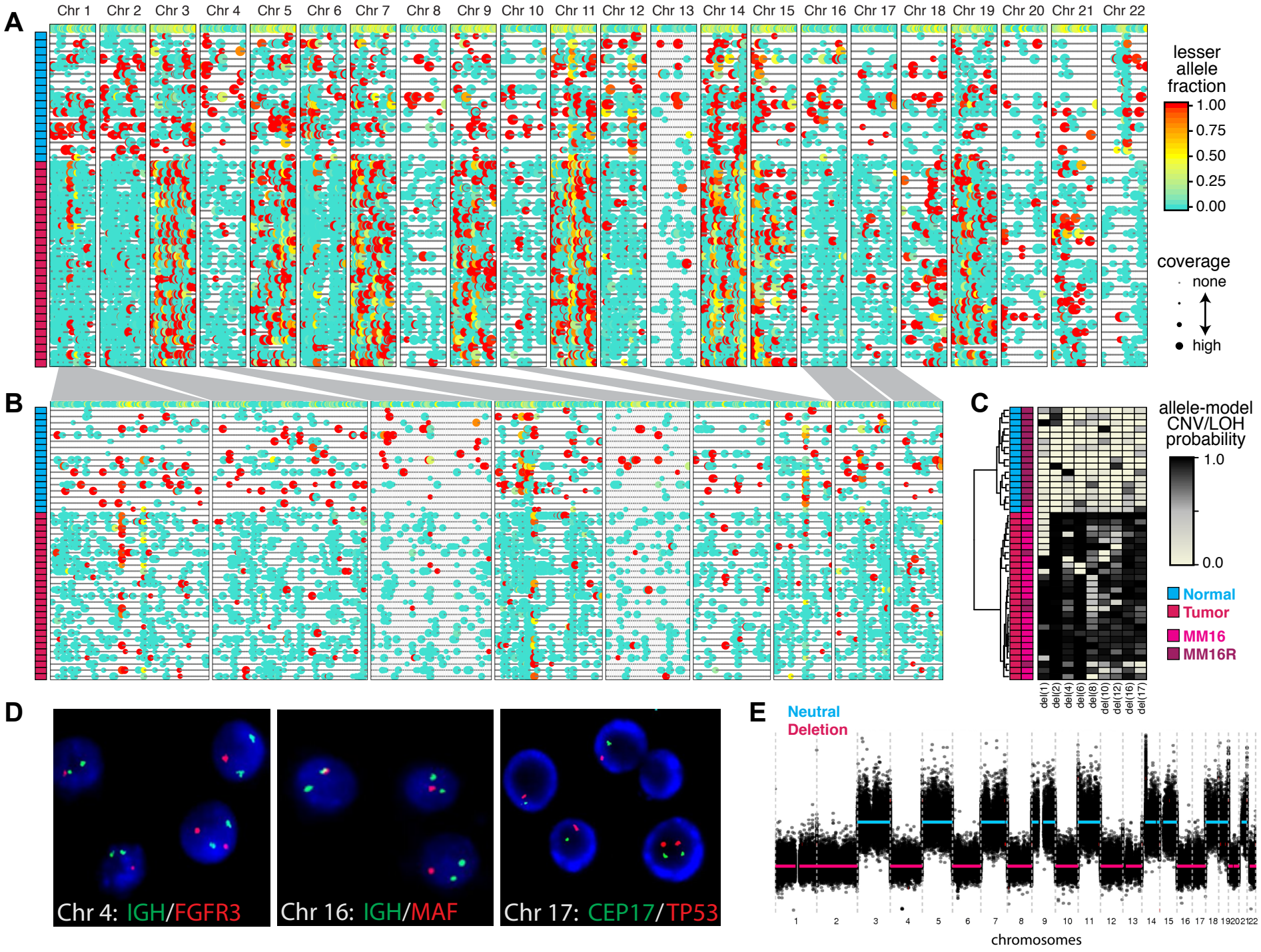
A
Chr 1
Chr 2
Chr 3
Chr 4
Chr 5
Chr 6
Chr 7
Chr 8
Chr 9
Chr 10
Chr 11
Chr 12
Chr 13
Chr 14
Chr 15
Chr 16
Chr 17
Chr 18
Chr 19
Chr 20
Chr 21
Chr 22
lesser allele fraction
1.00
0.75
0.50
0.25
0.00
coverage
none
high
B
C
allele-model CNV/LOH probability
1.0
0.0
Normal
Tumor
MM16
MM16R
del(1)
del(2)
del(4)
del(6)
del(8)
del(10)
del(12)
del(16)
del(17)
D
Chr 4: IGH/FGFR3
Chr 16: IGH/MAF
Chr 17: CEP17/TP53
E
Neutral
Deletion
1
2
3
4
5
6
7
8
9
10
11
12
13
14
15
16
17
18
19
20
21
22
chromosomes

Fig. 4

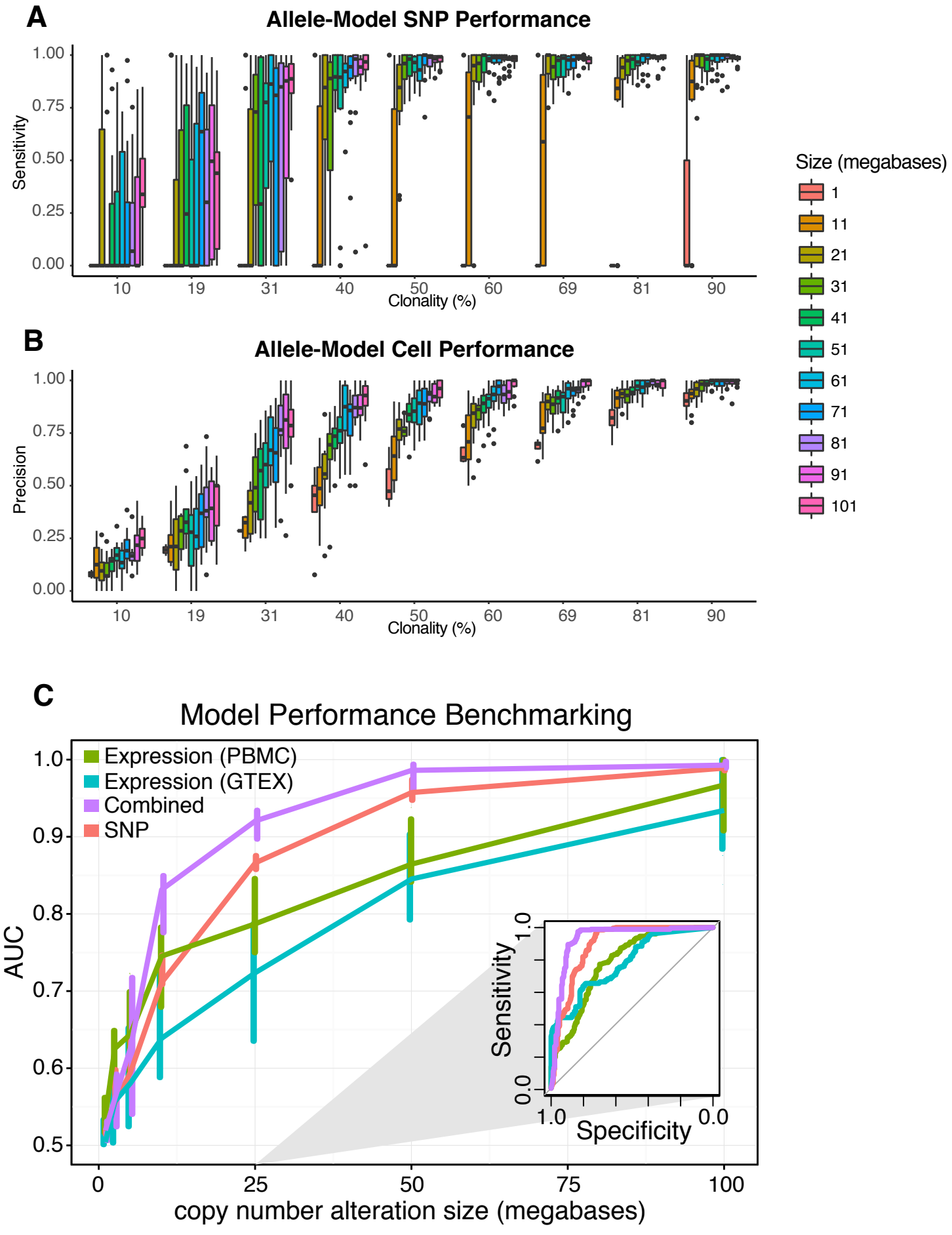

Fig. 5

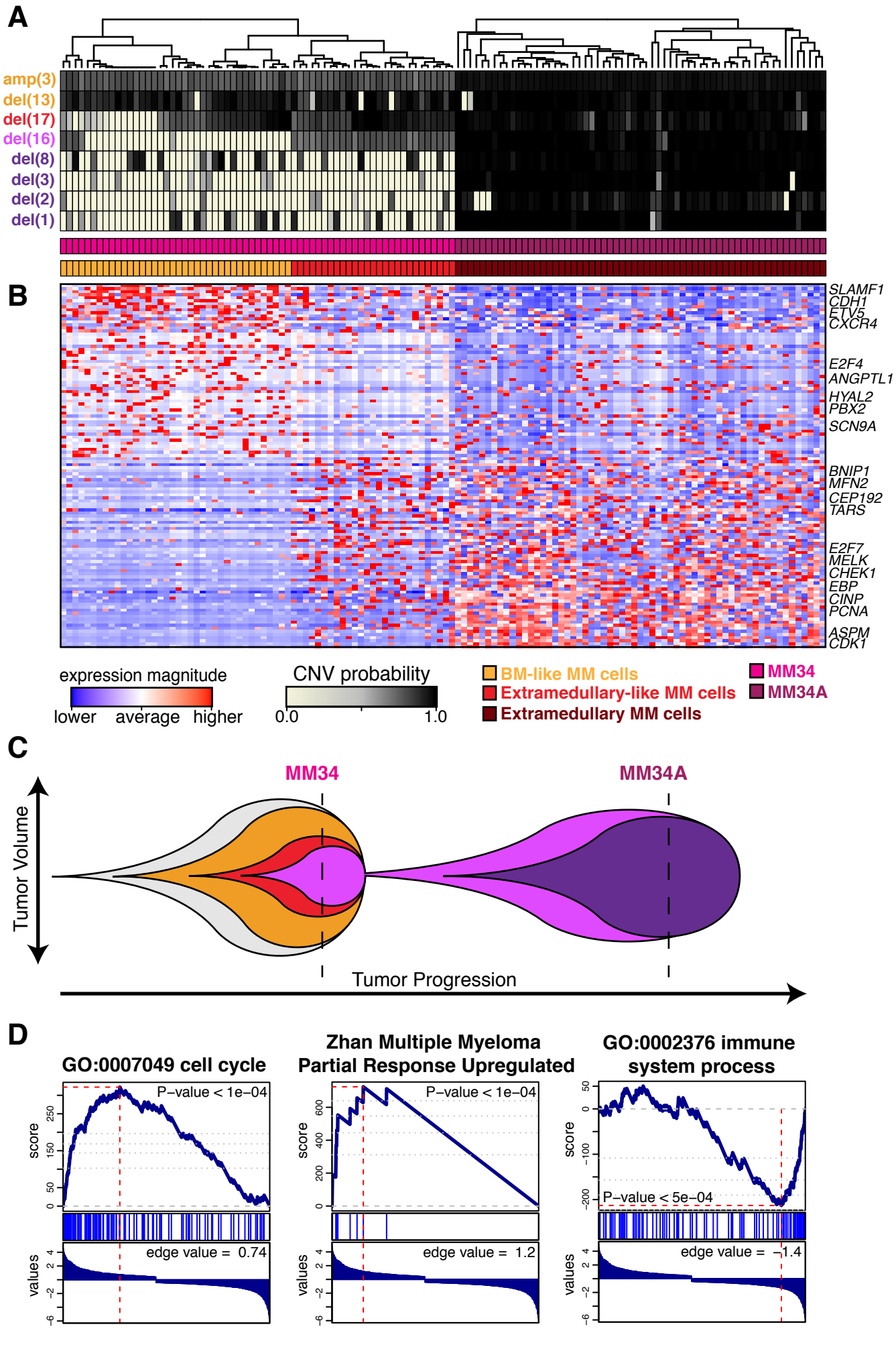

Fig. 6

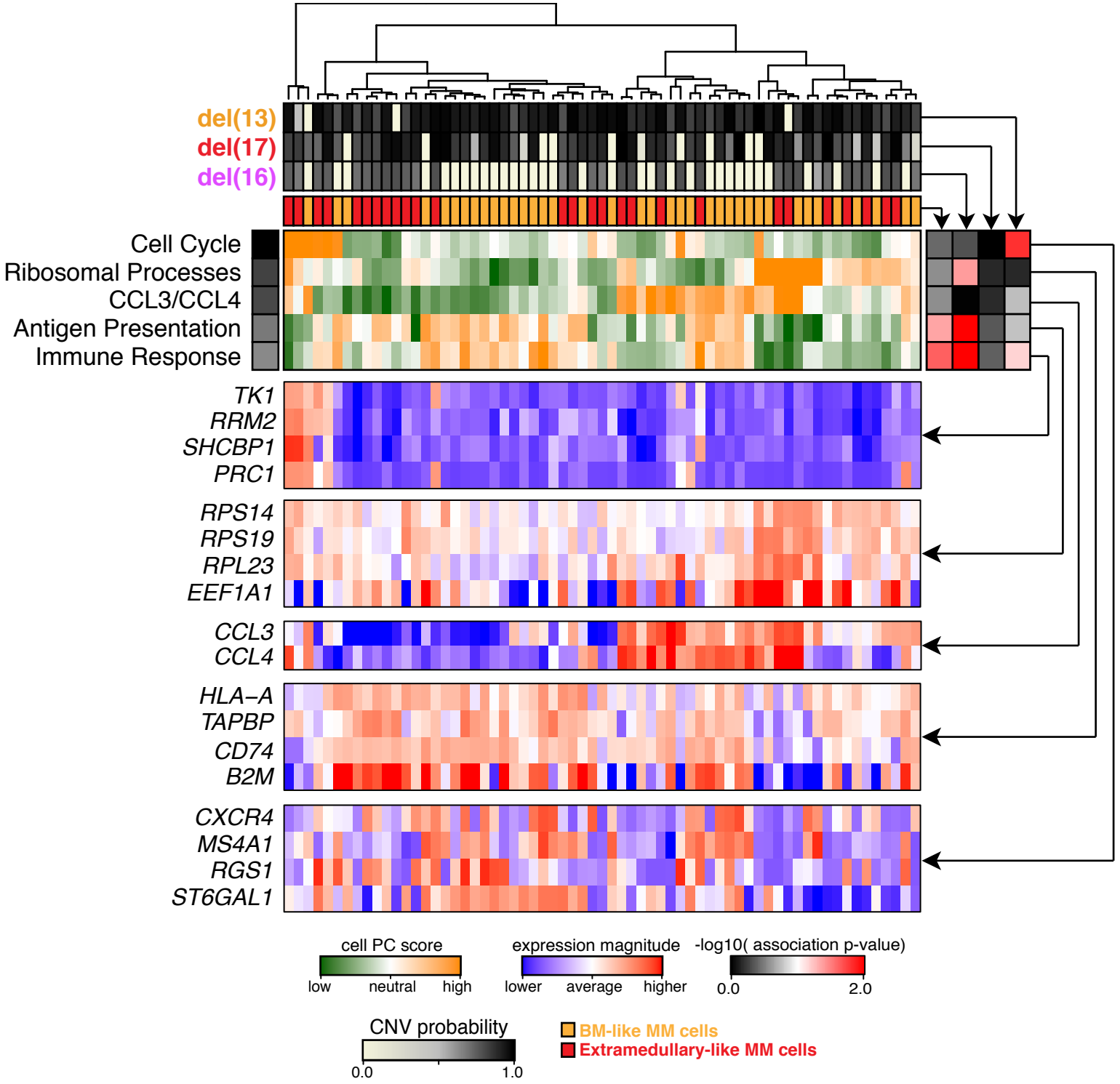

Linking transcriptional and genetic tumor heterogeneity through allele analysis of single-cell RNA-seq data

Jean Fan, Hae-Ock Lee, Soohyun Lee, et al.

Genome Res. published online June 13, 2018
Access the most recent version at doi:10.1101/gr.228080.117